buildings

MDPI

Article

Multiscale Hygrothermal Assessment of Bio-Fiber-Reinforced Materials for Energy-Efficient Building Envelopes

Kenza Sidqui, Yousra Taouirte, Michael Marion, Ionut Voicu, Anne-Lise Tiffonnet and Hasna Louahlia *

LUSAC Laboratory, Université de Caen Normandie, Site Universitaire Bellevue, 120 Rue de L'exode, 50000 Saint-Lô, Manche, France; kenza.sidqui@unicaen.fr (K.S.); yousra.taouirte@unicaen.fr (Y.T.); michael.marion@unicaen.fr (M.M.); ionut.voicu@unicaen.fr (I.V.); anne-lise.tiffonnet@unicaen.fr (A.-L.T.)
* Correspondence: hasna.louahlia@unicaen.fr

Abstract

Earth-based materials are promising candidates for balancing thermal performance, hygrothermal regulation, and environmental sustainability. The objective of this study is to evaluate and compare the hygrothermal behavior of two earthen materials, structural cob and lightweight insulating earth, against conventional reference concrete, taking into account not only their insulating properties but also their ability to regulate coupled heat and moisture transfers. Experimental tests show a significantly higher hygroscopic buffering capacity for earth-based materials, with an MBV of 2.23 g/(m^2·%RH) for the structural material and 1.21 g/(m^2·%RH) for the insulation material, compared to less than 0.5 g/(m^2·%RH) for concrete. The sorption isotherms confirm distinct water storage behaviors, with an average sensitivity to relative humidity of 10.47% for the insulation material, compared to 3.8% for concrete and 2.25% for the structural material, in addition to an average reduction of 26% in the adsorption capacity between 23 °C and 45 °C for both earthen materials. Coupled heat–moisture simulations in COMSOL quantitatively demonstrate the hygrothermal superiority of bio-based materials over conventional concrete, as concrete promotes interstitial moisture accumulation due to its low vapor permeability. The parametric sensitivity analysis highlights the effect of hygrothermal properties, where diffusivity controls transport kinetics and sorption governs water storage, while thermal conductivity modulates the spatial redistribution of thermo-hygric fields. The next and final step made it possible to link the phenomena observed at the material scale to the actual energy performance of the building, confirming the potential of the double-wall cob + lightweight earth system to reduce heating and cooling requirements and maintain stable indoor comfort, where the annual heating demand is reduced by approximately 24% compared to the conventional prototype.

Keywords: earthen materials; low thermal conductivity; MBV; sensitivity analysis; transport properties; storage properties; double-layer wall; energy performance

Check for updates

Academic Editor: Ali Memari

Received: 7 May 2026
Revised: 11 June 2026
Accepted: 18 June 2026
Published: 21 June 2026

Copyright: © 2026 by the authors. Licensee MDPI, Basel, Switzerland. This article is an open access article distributed under the terms and conditions of the Creative Commons Attribution (CC BY) license.

1. Introduction

In a context where a reduction in energy consumption and carbon emissions has become an important matter for climate change mitigation and sustainable development, construction materials are one of the key parameters of energy balance. The construction sector contributes approximately 36% of the global energy consumption [1] and 39% of carbon dioxide emissions in 2018 [2]. This makes the decarbonization of buildings through

their entire life cycles a major research goal. It is from this perspective that bio-based materials emerged, combining performance, sustainability, and low environmental impact [3]. Their potential is not limited to reducing the carbon footprint, as their complex physical behavior is strongly governed by their composition and porous structure. As mentioned by Latapie et al. [4], bio-sourced materials have a nonlinear hygroscopic interaction marked by hysteresis phenomena between absorption and desorption due to their porosity and raw materials, allowing them to offer an adaptive capacity to temperature and humidity variations. These properties make their behavior intelligent and better performing than conventional materials. Bio-based insulation materials like hemp and straw have demonstrated better thermal properties and lower embodied carbon compared to conventional insulation [5].

Among these bio-based materials, those based on raw earth go back a long time to traditional construction, making them capable of delivering a good performance [6]. This has led to the renewed interest and popularity of traditional earth buildings today, where many researchers have started studying and confirming their remarkable properties and affordability due to their local availability and recyclability [7,8]. Offering more sustainable and healthier construction, with the use of compressed earth blocks, rammed earth, adobe blocks, cob, etc., Hamard et al. [9] presented the role of earth construction techniques, particularly cob, as a solution for reducing the environmental impact of the building sector. They are also characterized by better thermal comfort, stability, and moisture-buffering capacities, improving indoor thermal comfort and passive heating and cooling [10]. Zeghari et al. [11] demonstrated the thermal potential of cob by maintaining interior temperatures down 6 °C from the exterior in summer. Experimental measurements on unfired clay bricks incorporating barley straw, hemp shiv, and corn cob show that these composites consistently achieve an excellent moisture buffering capacity superior to 2 [g/(m^2·%RH)] [12]. Other studies reported that raw earth with 10% hemp shives offers an MBV up to 3.16 [g/(m^2·%RH)], in addition to lowering the thermal conductivity by a factor of four, confirming the hygrothermal potential of these composites [13].

In modern earthen architecture, the aim is to develop a construction technique that combines both the mechanical role and insulation role, which can be achieved with optimized composition and reinforcement by natural fibers, improving the toughness and strength of earthen materials [14]. Several studies show the significant mechanical gain that the use of fibers can provide [15]. They can increase the open porosity, useful for sorption, and lower thermal conductivity [16]. The literature indicates that reed fibers have a good thermal performance, with the ability to reduce mortar's density by 75 kg/m^3 and elevate its porosity and adsorption capacity by 1.5%. But they did not improve the compressive or flexural strengths [17]. Therefore, the need arises to find complementary material solutions that ensure both mechanical and thermo-hygric performance. This is one of the main challenges accepted by the European CobBauge project, aiming to develop building materials based on local raw earth and natural fibers and providing better comfort, durability, and low environmental negative effects [18]. The CobBauge project redesigned the use of cob via a double-layer wall combining structural cob on the inside and lightweight insulating earth on the outside. The carefully studied design of the mixtures makes it possible to achieve the required mechanical properties while maintaining a good thermal performance and desired vapor permeability [19].

Despite these advantages, earth-based materials still present challenges that are the main target of researchers, including limited data on performance [20], variability of their properties and complex behaviors making their characterization and dimensioning difficult, particularly regarding moisture regulation. Their hygroscopic behavior remains poorly documented compared to conventional materials such as concrete or mortar. Controlling

moisture behavior is crucial, as it is one of the main causes of envelope degradation. It can lead to water vapor condensation, mold growth, structural damage [21,22], reduced thermal insulation [23], and deterioration of indoor air quality [24], which can adversely affect the comfort and health of occupants [25]. However, understanding this behavior cannot be reduced to static analysis while heat and moisture transfer through walls are intrinsically coupled. Numerical investigations applied to renovated walls in humid climates showed that peaks in moisture content within the insulation layers can cause increases in thermal transmittance of more than 22% compared to dry state values [26], which will cause additional transmission losses at the building scale. Bucklin et al.'s work showed that in hygroscopic bio-based materials, moisture absorption alone can increase thermal conductivity by 20% [27]. Thus, ignoring moisture dynamics systematically underestimates actual heat loss. When the coupling is properly modeled, hygroscopic materials can reduce heating and cooling consumption by 5 to 30% by attenuating indoor humidity variations through latent heat effects [28]. Beyond energy consumption, excessive moisture triggers biological degradation processes. Mold growth begins between 80 and 95% relative humidity depending on temperature, exposure time, and the nature of the material [29]. Given these challenges, a multiscale approach can be beneficial as each scale captures phenomena that the others cannot. At the material level, experimental tests provide the essential input parameters. Coupled heat–air–moisture (HAM) transient simulation captures latent heat effects, dynamic variations in thermal transmittance, and moisture-related risks that cannot be obtained by a static calculation. At the building scale, dynamic energy simulation evaluates the overall impact on heating and cooling consumption.

Many literature reviews present hygrothermal data [30], but provide an incomplete understanding of the actual contribution of each of the properties. This justifies the need for sensitivity analyses focused on transport/storage parameters to identify the dominant levers and quantify their effect on heat distribution and water content. This work has two objectives. The first is to experimentally characterize the two earth-based materials based on their physical and hygroscopic properties, and then to compare their behavior with that of a conventional reference material, concrete. The second objective is to numerically analyze the influence of the main thermo-hygric properties on changes in water content, in order to identify the parameters governing transfer kinetics, moisture storage capacity, and the redistribution of thermo-hygric fields within the material. Finally, to go beyond the material-level scale, this study also seeks to assess the extent to which the observed behaviors can translate into benefits at the building scale, through dynamic energy simulation of a prototype incorporating these materials.

2. Measured Thermal and Hygric Properties of the Studied Materials

2.1. Materials

Two materials were studied: a bio-based structural material and an insulating material, and were compared to a conventional reference, concrete. Their thermal and hygric properties were collected from experimental data presented in previous work [31–33] and from the literature for concrete [34]. (The reference values for concrete presented for comparison are derived exclusively from the literature and are mentioned solely to provide context for the results obtained.) These properties are essential inputs for modeling, as they govern the kinetics of vapor transport, storage capacity and thermal response. Each has a specific porous architecture and composition, reflecting how it stores, exchanges and transfers heat and moisture. The materials' properties are presented in Table 1.

The bio-based materials studied are materials from the European CobBauge project, whose first phase consisted of developing earth-based materials reinforced with fibers for construction purposes, with the aim of achieving better energetic performances, a low

carbon footprint and occupants' comfort. This phase ended with the development of two materials with distinct roles: a structural material as the load-bearing material, which consists mainly of cob and a low percentage of straw fibers, while the insulation consists of a high percentage of reed fibers and lightweight earth (Figure 1).

Table 1. Material properties.

Properties	Structural [31–33]	Insulation [31–33]	Concrete [34]
Thermal conductivity [W/(m·K)]	0.295	0.104	2.74
Specific heat [J/(kg·K)]	832	1090	940
Density [kg/m^3]	1492	541	2200
Water vapor permeability [Kg/(m·s·Pa)]	3.53×10^{-11}	3.14×10^{-11}	4.54×10^{-12}
Diffusion coefficient [m^2/s]	4.09×10^{-9}	1.44×10^{-9}	2.19×10^{-10}
Porosity [-]	0.30	0.64	0.16



(**a**) (**b**)

Figure 1. Pictures of the earthen materials studied: (**a**) insulation; (**b**) structural.

The structural material consists of a mixture of two soils: raw sand (50%) and brown silt (100%); these proportions were determined to ensure sufficient mechanical strength. These soils were first dry-mixed to ensure a homogeneous distribution. Water was gradually added up to 20% of the dry mass of the soil mixture. The mixture was kneaded until a homogeneous and uniform consistency was obtained. Flax straw fibers were incorporated at a percentage of 2.5% to reinforce the mixture. They were incorporated gradually in small quantities by trampling the mixture, ensuring a uniform incorporation.

The preparation of the insulation material consisted of mixing the lightweight soil with 80% water by weight of its dry mass, and the mixture was left to rest. The reed fibers (50% of soil dry mass) were then incorporated manually in small quantities to ensure homogeneity. The mixtures were then poured into molds of defined dimensions and left to dry.

The selected fiber contents for the materials studied were determined based on previous studies [35] that identified the optimal balance between mechanical strength and thermal performance. An increase in fiber percentage improves insulating properties by reducing bulk density, but leads to a significant decrease in compressive strength, with mixtures with 5% fibers for the structural material generally falling below the 0.9 MPa threshold required for two-story constructions.

Based on the parameters of the different materials presented in Table 1, the structural material with a 30% porosity combines a higher permeability, and thus a high diffusivity, which can therefore allow it to exchange and equilibrate quickly, making it a good short-term buffer. The insulation, with a higher sorption capacity, has a low density and high porosity, promoting surface exchanges, with internal variations occurring slightly more slowly than with the structural material. However, concrete has the highest vapor resistance, which can cause more moisture accumulation under a vapor gradient. Regarding thermal

conductivity, the insulation has higher thermal resistance, slowing down the heat transfer throughout the material.

2.2. Moisture Buffering Value

To analyze the role of materials in regulating indoor humidity, the Moisture Buffer Value (MBV) was measured, as it serves as a key indicator of materials' ability to moderate humidity fluctuations in the built environment. Tests were conducted using the NORDTEST standard method [36] to characterize their hygroscopic behavior through humidity and mass variation measurements. One sample per material was prepared with an exchange surface area equal to 103.5 cm^2 ($\pm$0.5 mm), in accordance with the protocol's minimum requirements.

The test specimens were manufactured according to the formulation protocol described in Section 2.1, ensuring the homogeneity of the composition and microstructure. Prior to testing, the samples were dried in an oven at 40 °C until a constant mass was achieved (criterion: mass variation less than 0.1%/24 h). The literature shows that the drying temperature and duration influence the initial water content of samples but do not significantly affect the obtained MBV value, with an observed difference of less than 1% [37,38]. The samples were sealed with aluminum tape on all the side surfaces, except for the top one, to ensure unidirectional heat and moisture transfer during the tests (Figure 2). Then, they were placed on a precision balance with a 0.001 g sensitivity, inserted in a climatic chamber. The climatic conditions were set at 50% relative humidity and 23 °C until the samples' mass variation fell below 0.1%/24 h.

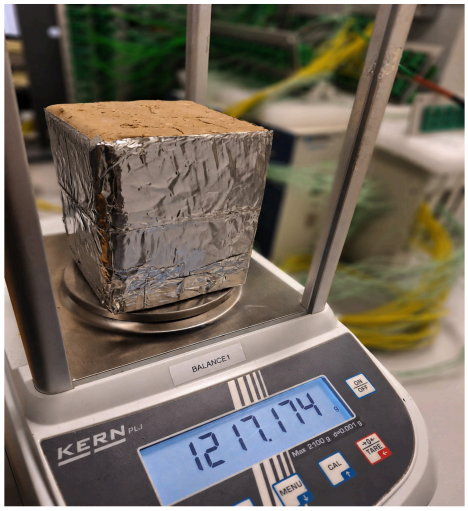


Figure 2. The structural material sample used in the MBV experiment test.

The NORDTEST protocol cycles were then applied. During the 24 h cycle, humidity is set to 33% for 16 h and then to 75% for 8 h, at a constant temperature of 23 °C. Cycles are repeated over several days, and the instantaneous mass of each sample was monitored and recorded throughout the test. The test was maintained until the equilibrium condition defined by the protocol had been reached, corresponding to a mass variation of the samples of less than 5% during the last three cycles.

To verify that the thickness of the samples is sufficient for the MBV to be an intrinsic property, the penetration depth pd was estimated using Equation (1) [39,40]:

$$\mathrm{pd} = 4.61 \cdot \sqrt{\frac{D_w \cdot t}{\pi}} \quad (1)$$

where D_w is the moisture diffusivity (m^2/s) and t is the period of the shortest exposure phase (s).

For the structural material, the estimated penetration depth is pd = 2.82 cm, and it is 1.67 cm for the insulation. These values are lower than the thickness of the samples, which is equal to 11.5 cm, confirming that the condition is satisfied and that the measured MBVs are indeed intrinsic properties of the materials, independent of the thickness of the samples.

The moisture buffering value [$g/(m^2 \cdot \%RH)$] of each material is obtained from the mass variation measured at the end of the adsorption and desorption cycles during the last five stabilized cycles. MBV is calculated using Equation (2):

$$MBV = \frac{\Delta m_{sample}}{A\left(\phi_{High} - \phi_{Low}\right)} \quad (2)$$

In this equation, Δm_{sample} [g] is the average between the absorbed and released water contents during the last cycles, A [m^2] is the exposed surface area, and ϕ_{High} and ϕ_{Low} [%] are the high and low relative humidity values occurring during the cycles.

The time variation in the masses of the structural and insulation samples during the tests is shown in Figure 3. A significant increase in mass is observed during the first three cycles. After the fourth cycle, a slight increase in mass is observed during the adsorption and desorption cycles, which may indicate that the samples can store moisture in an almost stable manner. The required stationary state is obtained for cycles 4–8, as the mass variation is less than 5% and the difference between the weight gain and the weight loss in each cycle is less than 5%.

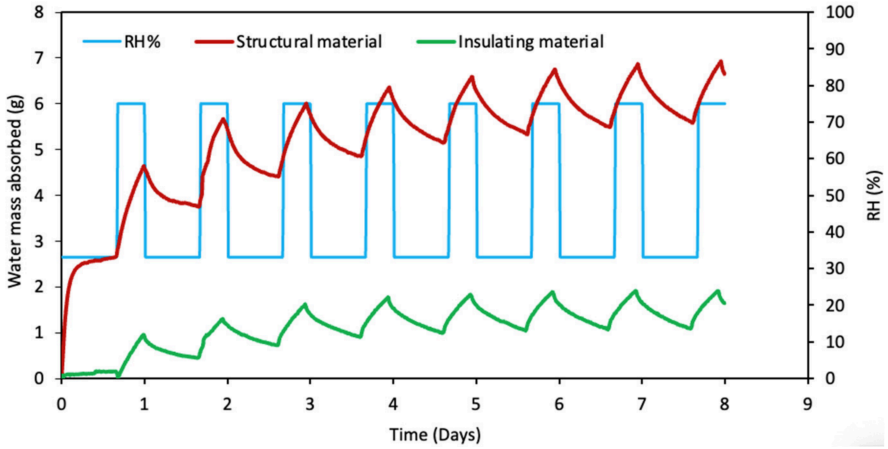


Figure 3. Absorbed mass variation of the structural and insulation materials during the eight adsorption cycles.

An assessment of temporal repeatability was performed by calculating the MBV independently for each of the stabilized cycles, providing a direct estimate of cycle-to-cycle variability under identical experimental conditions. For the structural material, the average desorption MBV is 2.158 ± 0.069 [$g/(m^2 \cdot \%RH)$], and during adsorption, it is 2.292 ± 0.057 [$g/(m^2 \cdot \%RH)$]. For the insulating material, the average MBV during desorption is 1.233 ± 0.032 [$g/(m^2 \cdot \%RH)$], and during adsorption, it is 1.192 ± 0.055 [$g/(m^2 \cdot \%RH)$].

The NORDTEST protocol provides a scale that interprets the results by classifying the values into levels, as shown in Figure 4. The structural material can be considered an "excellent moisture regulator", with an MBV of 2.23 ± 0.032 [$g/(m^2 \cdot \%RH)$]. The insulation material has an MBV of 1.21 ± 0.017 [$g/(m^2 \cdot \%RH)$], which makes it a "good moisture regulator", as is the case for spruce wood, with an MBV higher than 1 [$g/(m^2 \cdot \%RH)$]. Other

common materials such as concrete and brick have an MBV of less than 0.5 [g/(m^2·%RH)], and are thus considered "weak moisture regulators" [36]. These results fall within the ranges reported in the literature for comparable materials. The structural material is consistent with the values for earthen materials and hemp–clay composites, for which MBVs ranging from 1.9 to 3.4 [g/(m^2·%RH)] have been documented [39,41,42]. The insulation material also falls within the same range as bio-based insulators such as wood fiber (1.61 [g/(m^2·%RH)]), grass (1.79 [g/(m^2·%RH)]) as well as spruce wood, as mentioned earlier [43]. These results confirm the good hygroscopic properties of earth-based materials and their suitability for passive indoor humidity control.

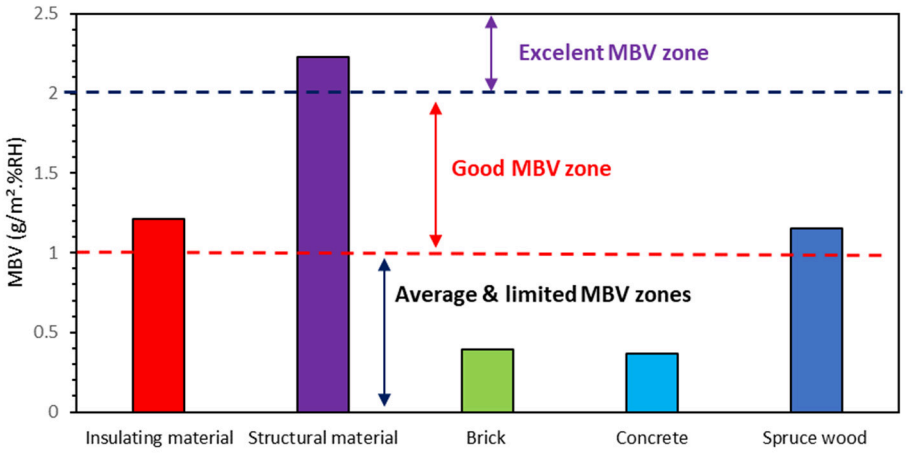


Figure 4. Moisture buffer values of earthen materials and other building materials.

2.3. Sorption Isotherms

To model the sorption capacity of the materials under study, the Guggenheim–Anderson–de Boer (GAB) model was fitted using experimental data from sorption tests conducted at different relative humidity levels in the climatic chamber. For each specified humidity level, the samples were held until a state of mass equilibrium was reached, that is, until their mass stabilized. The equilibrium mass obtained at each relative humidity level was then used to determine the material's equilibrium water content, expressed in kg of water per kg of dry material [kg/kg].

$$W = \frac{w_w \cdot K \cdot C \cdot \phi}{(1 - K \cdot \phi)(1 - K \cdot \phi + C \cdot K \cdot \phi)} \quad (3)$$

where w_w, C and K represent the fitting parameters of the GAB model. Relative humidity ϕ is calculated as a fraction in the equation.

The GAB model was fitted using MATLAB's (R2025b) Curve Fitter tool. This procedure allowed for the estimation of the model parameters, making it possible to quantitatively describe the sorption behavior of the studied materials over the considered relative humidity range, by establishing a relationship between the hygrometric environment and the material's water storage capacity.

To evaluate the GAB model's ability to accurately represent the sorption behavior of the materials studied, an analysis of the fit accuracy was performed by comparing the experimental water content values with those predicted by the model. The quality of the fit was quantified using statistical indicators commonly used in the analysis of nonlinear models, notably the coefficient of determination R^2 and the root mean square error $RMSE$. A high value of R^2, close to 1, combined with a low RMSE value, indicates that the GAB model is capable of accurately reproducing the experimental data and describing the relationship between water activity and the material's water content. This is the

case for the fitted model in this study, where $R^2 = 0.9959$, $RMSE = 0.002$ kg/kg and $R^2 = 0.9975$, $RMSE = 0.007$ kg/kg respectively for the structural and insulation materials, demonstrating a good fit for both materials.

Results are gathered in Table 2, representing the values of the fitting parameters w_w, C and K. Figure 5 shows the sorption isotherms for the structural and insulation materials studied in this work, compared with the concrete sorption isotherm taken from the literature [34]. The position of the concrete curve between those of the structural material and the insulation material reflects the physical differences in water storage capacity between these materials. Bio-based and fibrous insulation materials generally have high porosity, promoting water vapor adsorption and leading to higher water contents for a given relative humidity. The structural material, on the other hand, has a lower moisture storage capacity than concrete itself.

Table 2. GAB fitting parameters.

Material	w_w	C	K
Structural	0.0096	2.104	0.6639
Insulation	0.033	2.5218	0.7683
Concrete	0.0108	13.503	0.8023

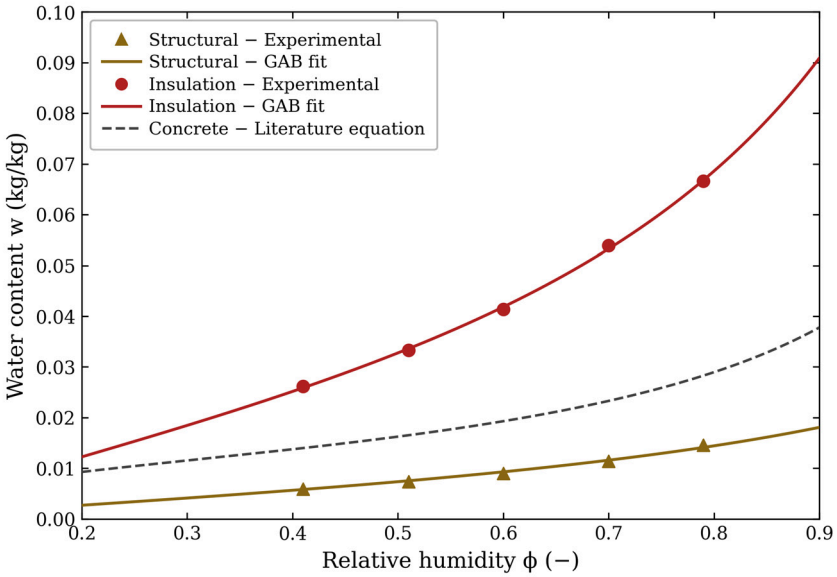


Figure 5. Comparison of GAB sorption isotherms of the bio-based and conventional materials.

2.4. Effect of Temperature and Relative Humidity on Water Vapor Accessible Porosity

Water vapor accessible porosity refers to the amount of accessible void space within a material's volume capable of participating in adsorption, capillary condensation, and water transport phenomena under given temperature and relative humidity conditions, making it a relevant indicator for interpreting the hygrothermal behavior of porous materials. The method used to measure this indicator consists of a sorption test in the climatic chamber, under various temperature and relative humidity conditions. The samples were exposed to relative humidity levels varying from 40 to 80% at three temperatures (23 °C, 30 °C, and 45 °C). It is calculated as the ratio of the volume of water vapor absorbed V_w to the total apparent volume of the material V_t:

$$\varepsilon_w(-) = \frac{V_w}{V_t} \quad (4)$$

where V_w is determined from the difference between the mass at a given relative humidity and the dry mass of the material divided by water density (1000 kg/m^3). V_t is the total apparent volume of the sample determined from its external dimensions.

Two consistent trends are observed for both materials: ε_w increases with relative humidity, reflecting the progressive filling of the pores as vapor pressure increases. However, it decreases with increasing temperature at the same relative humidity, with an average reduction of 26% between 23 °C and 45 °C. These findings are in accordance with the literature on earthen and bio-based materials, which report a reduction of 12% between 15 °C and 35 °C [44]. This behavior can be attributed to changes in vapor–liquid equilibrium within the pores.

The results shown in Figure 6 indicate that the insulating material has higher water vapor accessibility than the structural material. For the insulation, ε_w ranges from 0.83% to 3.20% compared to 0.54% to 2.14% for the structural material. This difference can be explained by the high fiber content of the insulation material, inducing a high porosity percentage and a lower bulk density, thus promoting a greater water vapor retention capacity.

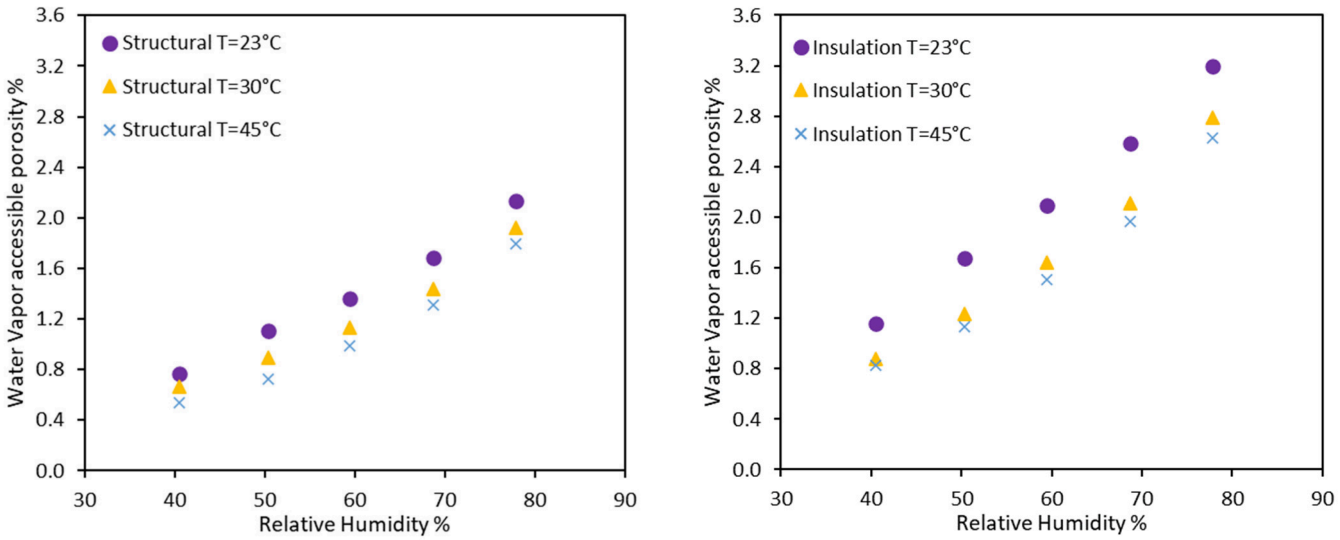


Figure 6. Impact of temperature and relative humidity variations on water vapor accessible porosity.

3. Comparative Analysis of Coupled Heat and Moisture Transfer in Bio-Based and Conventional Materials

3.1. Numerical Methodology

The numerical approach is based on the coupled modeling of heat and moisture transfer in porous materials, performed in COMSOL Multiphysics 6.3, using the Heat and Moisture Transport in Porous Media physics. This interface combines two physics: Heat Transfer in Moist Porous Media and Moisture Transport in Porous Media, to model simultaneously thermal conduction, vapor diffusion, and liquid water transport within the porous media, considering the latent heat effects related to condensation/evaporation dynamics. These physics were chosen over the Building Materials physics to obtain a more accurate representation of the actual behavior of the bio-based earthen materials, whose porous structure and hygroscopic behavior require a multiphase description. The governing partial differential equations of the coupled heat and moisture transfer are presented in Appendix A. The assumptions associated with these physics are as follows: terms related to capillary flow of liquid water and convection are neglected; thermal conductivity λ and vapor permeability δ_p are considered constant for each material, independent of water

content and temperature; and the local water content is assumed to be in instantaneous equilibrium with relative humidity, in accordance with the measured sorption isotherms.

The geometry studied is a 2D domain (Figure 7). The dimensions of the geometry under study are 10 × 10 cm^2, and the sample was simulated over 10 days in order to capture the transient response specific to each material. The impact of the time step on the simulation was evaluated by comparing three values: 30 s, 60 s, and 600 s. The results obtained showed no variation in the temperature nor the relative humidity maxima and minima, indicating full convergence of the hygrothermal solution. Furthermore, the computation time ranges from 58 s for a 600 s time step to 7 min 47 s for a 30 s time step, a factor of 8 with no gain in accuracy. A 60 s time step was therefore selected for all simulations, with a computation time of 4 min 18 s.

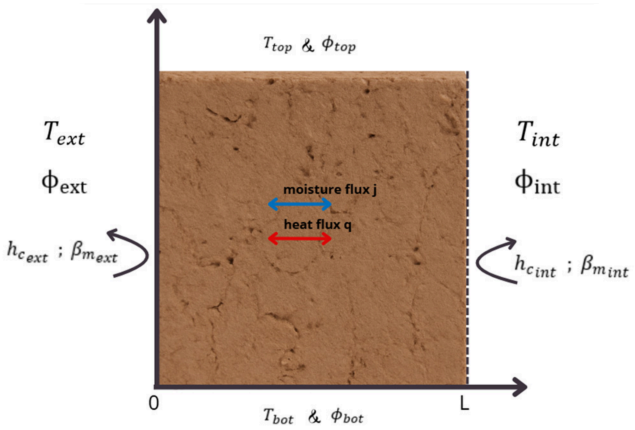


Figure 7. Model geometry and applied boundary conditions.

A mesh independence analysis was performed using three Physics-controlled mesh levels: Fine, Extra Fine, and Extremely Fine. As shown in Table 3, the maximum and minimum temperatures and the maximum and minimum relative humidity show negligible variation due to changes in mesh size. Since the Extremely Fine mesh significantly increased the computation time without yielding significant improvements in the results, the Extra Fine mesh was selected for the study.

Table 3. Mesh independence study.

Mesh Level	Number of Elements	T_{max} °C	T_{min} °C	ϕ_{max} %	ϕ_{min} %	Simulation Time
Finer	1856	11.166	5.4841	86.785	72.598	2 min 10 s
Extra Fine	6282	11.165	5.4839	86.824	72.569	4 min 18 s
Extremely Fine	24,912	11.165	5.4841	86.812	72.578	11 min 33 s

Table 4 presents the different parameters of the model. The boundary conditions are constant, where the exterior side is exposed to harsh and humid winter conditions and the indoor conditions were chosen below the comfort range, thereby evaluating the hygrothermal performance of the materials under critical conditions. The upper and lower boundary conditions represent the conditions of adjacent unheated spaces. The initial conditions (T_0, RH_0) correspond to a homogeneous state of the material prior to exposure, an assumption that ensures numerical stability and reproducibility of results. For the heat and water vapor diffusion transfer coefficients, typical values were considered following EN 15026:2023 [45]. This choice of conditions imposes a sustained thermal and hygric gradient, representative of a cold and humid period, which is conducive to revealing the mechanisms of vapor and water diffusion and possible episodes of moisture accumulation.

This simulation was applied successively to the three materials studied, in order to compare their hygrometric behavior under the same conditions.

Table 4. Model parameters.

Boundary Conditions (Critical Winter Conditions)			**Heat Transfer Coefficients (EN 15026:2023 [45])**		
T_{ext}	Exterior temperature	4 °C	$h_{c_{ext}}$	Heat transfer coefficients	17 W/(m^2·K)
T_{int}	Interior temperature	13 °C	$h_{c_{int}}$		8 W/(m^2·K)
ϕ_{ext}	Exterior relative humidity	95%	$\beta_{m_{ext}}$	Vapor diffusion transfer coefficients	75×10^{-9} s/m
ϕ_{int}	Interior relative humidity	65%	$\beta_{m_{int}}$		25×10^{-9} s/m
$T_{top,bot}, \phi_{top,bot}$	Top and bottom conditions	(10 °C, 75%)	T_0, RH_0	Initial conditions	(4 °C, 50%)

The indoor surface heat transfer coefficient $h_{c_{int}} = 8$ W/(m^2·K) takes into account the convective and radiative components. This standard value [45] corresponds to low indoor convection conditions (air velocity ≈ 0.1 m/s). It should be noted that air velocity has a significant impact on the moisture buffering capacity of hygroscopic materials: A study [37] has shown that the MBV of bio-based materials increases, for thermo-hemp, from 2.09 to 4.34 g/(m^2·%RH) with increasing air velocity from 0.099 m/s to 0.981 m/s. The moisture regulation performance presented in this study is therefore a conservative estimate, as higher air velocities lead to even more effective regulation.

3.2. Model Validation

To verify the reliability of the hygrothermal numerical model developed in COMSOL Multiphysics, an experimental validation was conducted by comparing numerical results with the experimental data from previous work [33]. These results were obtained from 7 cm cubic samples of structural and insulating material in a wet cup experimental setup. Each sample was preconditioned and tested at ambient temperature for 6 days until it reached the hygric steady state. The relative humidity was fixed at 80% in the bottom ambient environment. Relative humidity is recorded during the experiments at four experimental points within the materials: on upper and lower surfaces of the sample and inside the material at 2 cm and 5 cm from the lower surface. Figure 8 shows that the water content distribution is in close agreement with the numerical water content, with an RMSE of 0.1401 kg/m^3 for the insulation and 0.8694 kg/m^3 for the structural material, which indicates good agreement between the numerical results and the experimental data, confirming the model's ability to accurately reproduce the behavior of the studied materials.

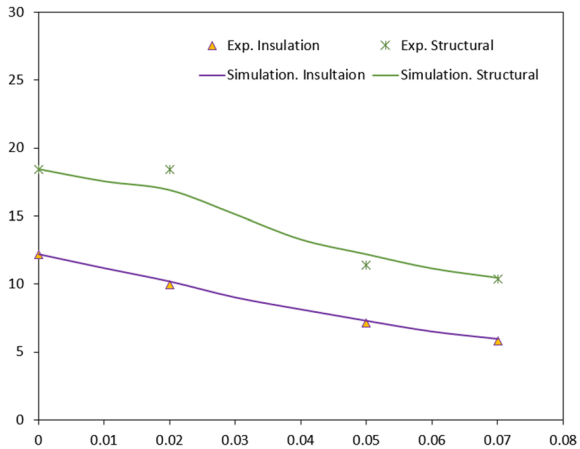


Figure 8. Model validation through water content distribution across the earthen samples.

3.3. Thermo-Hygric Behavior of Bio-Based and Conventional Materials

The objective of this section is to compare the thermo-hygric behavior of the three materials subjected to the same climatic conditions. Figures 9–11 show surface plots of the three materials, representing the spatial distribution of relative humidity. The line contours represent the temperature distribution, in addition to the maximum and minimum temperatures and relative humidities, respectively, in red and blue, after a 10-day simulation. The profiles for the three materials highlight marked differences in behavior related to their properties.

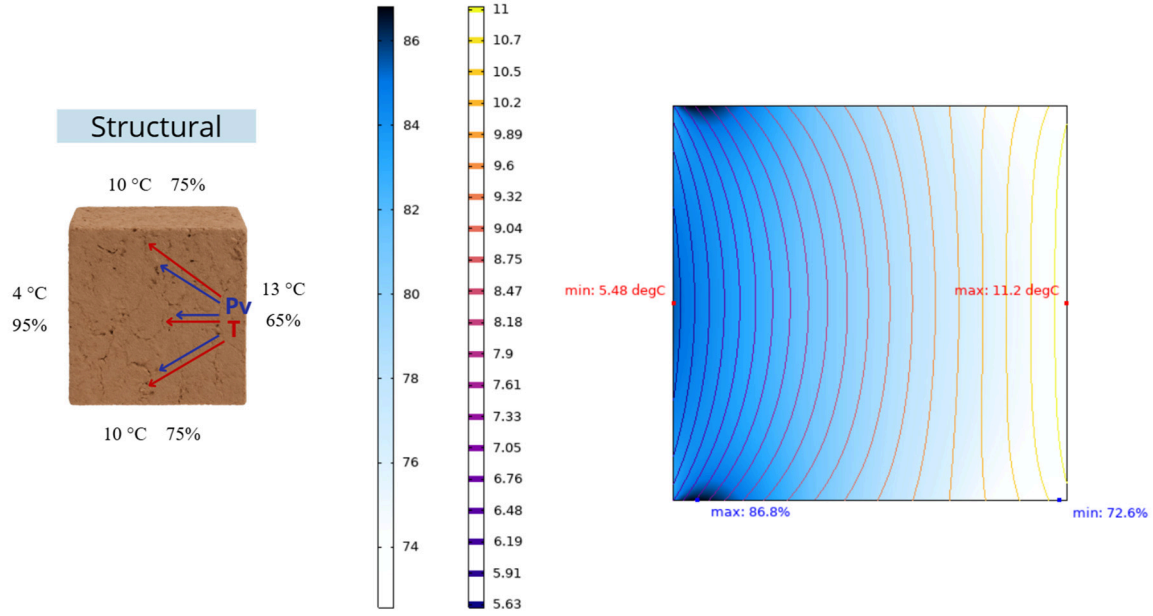


Figure 9. Thermo-hygric behavior of structural material under winter conditions.

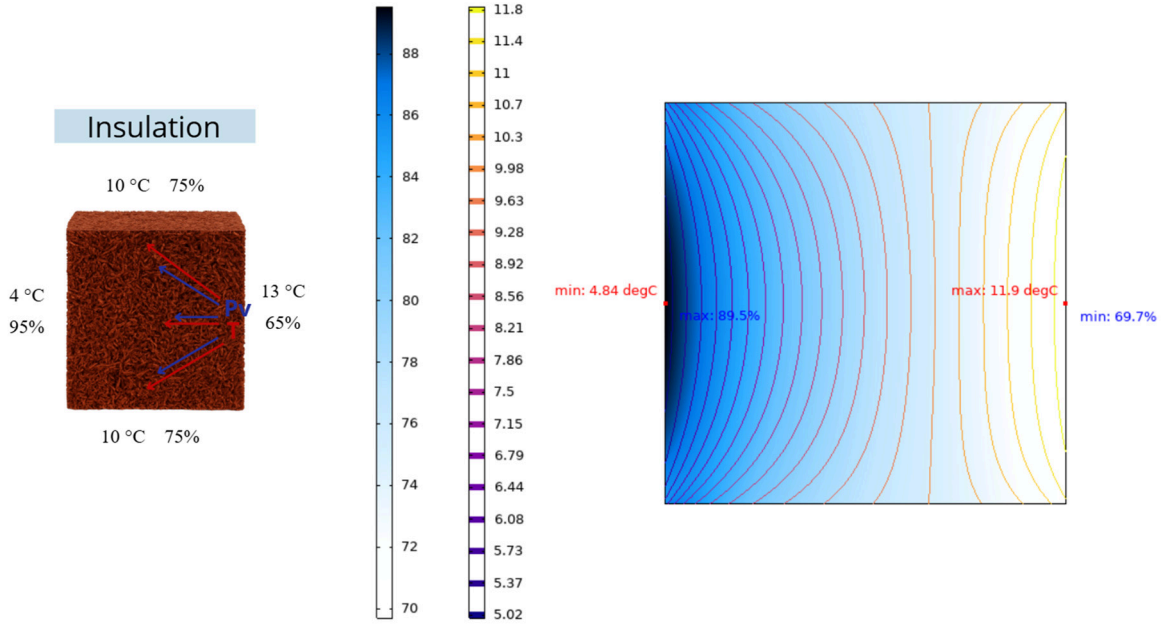


Figure 10. Thermo-hygric behavior of insulation material under winter conditions.

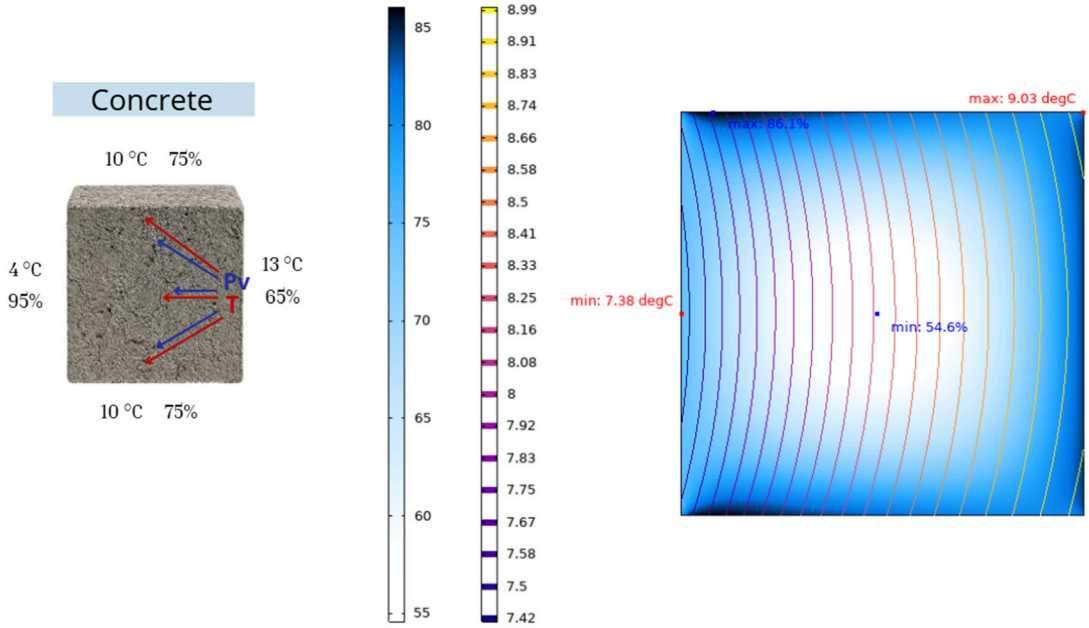


Figure 11. Thermo-hygric behavior of concrete material under winter conditions.

For the structural material in Figure 9, the temperature varies from a minimum of 5.48 °C to a maximum of 11.2 °C, showing a moderate gradient due to its intermediate thermal conductivity. Relative humidity ranges from 86.8 to 72.6% from the exterior to the interior, while the color map shows a progressive internal diffusion, showing the influence of the local temperature, without marked localized accumulation on either side. Small zones of high humidity are observed in the top and bottom cold corners. This can be explained by the corner effect, where the heat flux coming from the center of the material decreases approaching the corners, causing the moisture flux to encounter colder zones, and thus, with a decrease in p_{sat}, ϕ increases locally.

The insulation material (Figure 10), on the other hand, has a more marked temperature gradient, with a variation from 4.84 °C to 11.9 °C, which is due to its higher thermal resistance compared to the other two materials, reducing heat diffusion and thus fulfilling its role in slowing heat dissipation in order to maintain a warmer interior. A high vapor accumulation is observed on the cold side, which is favored by its high sorption capacity and a lower diffusion coefficient and permeability compared to the structural material. Furthermore, because the temperature on the exterior side remains lower, it results in a lower saturated vapor pressure and therefore a greater possibility of saturation along the exterior surface.

For concrete (Figure 11), the temperature ranges from 7.38 °C to 9.03 °C, which is the smallest difference, due to its high thermal conductivity. Heat diffuses quickly through the thickness, lowering the interior surface temperature. Its low diffusion coefficient indicates slow moisture diffusion, confirmed by the observed gradient, showing high heterogeneity of relative humidity throughout the sample. Moisture accumulation is observed at the outer corners and locally on the inner surface. This can be explained by the combination of higher vapor partial pressure p_v and low temperature. At the corners, heat escapes more easily, making the area colder than the rest. The local temperature drops, and thus, the saturated vapor pressure decreases, which makes the corners critical for condensation and mold growth. Regarding moisture accumulation on the interior surface, when heat migrates through the wall, the interior temperature drops faster than the vapor content can diffuse. This time lag can cause an apparent accumulation of ϕ on the interior side.

This confirms that the assumptions made based on the thermal and hygric properties of the studied materials are validated by these figures, demonstrating a better performance of the bio-based materials compared to concrete. The structural and insulation materials showed greater hygrometric regulation and buffering behavior, while concrete increases the risk of vapor accumulation indoors in cold conditions due to its lower vapor permeability and higher thermal conductivity.

3.4. Parametric Investigation of Coupled Heat and Moisture Transfer

In order to better understand the behaviors of the materials under study, this section provides a parametric decomposition aiming to analyze the influence of certain key properties on the performance and response of each material, which will help to identify and quantify each property's contribution to heat and moisture transfer.

Three parameters were separately varied to transition from observation to causation: diffusion coefficient, sorption capacity, and thermal conductivity. During these tests, everything else remained the same, as indicated in Section 3.1 (geometry, boundary conditions and other properties). The objective is to analyze the roles of each one of these parameters.

To analyze the spatial distribution of the hygrothermal fields within the material, three locations are considered across the thickness: the outer surface (x = 0), the center (x = 0.05 m), and the inner surface (x = 0.10 m).

3.4.1. Influence of the Diffusion Coefficient on Thermo-Hygric Behavior

The objective here is to isolate and analyze the influence of the diffusion coefficient on moisture transfer. Three simulations were conducted in which only the diffusion coefficient of the structural material was varied around its reference value, considering three distinct values: the reference case, a 50% increase, and a 50% decrease. The comparison is based on the water content variation.

The results presented in Figure 12 show that when the diffusion coefficient increases, and therefore the mass diffusivity as well (since the sorption capacity is constant here (Equation (5)), the water content curves rise more quickly, and the internal point catches up with the surface sooner. On the other hand, the equilibrium value does not change. The more the diffusivity coefficient increases, the more the slope increases, and the material arrives at a stable state more rapidly. The decrease from 6×10^{-9} m^2/s to 4×10^{-9} m^2/s results in a 34% increase in the stabilization time, which increases from 4.7 to 6.3 days. Similarly, the reduction from 4×10^{-9} m^2/s to 2×10^{-9} m^2/s results in a 54.8% increase in stabilization time, reaching 9.75 days. Despite these differences, the water content equilibrium value remains identical for all cases, confirming that the diffusion coefficient acts on the propagation and stabilization speed. This means that a higher diffusion coefficient reduces the internal humidity gradients, causing better moisture redistribution and a lower risk of accumulation.

$$D_w = \frac{D_m}{\xi} \tag{5}$$

where $D_m = \delta_p \cdot P_{sat}(T)$ and $\xi = \frac{\partial w}{\partial \varphi}$.

D_w $[m^2/s]$ is the diffusion coefficient, D_m $[kg/(m \cdot s)]$ represents the moisture diffusivity, δ_p $[kg/m \cdot s \cdot Pa]$ is the permeability, and ξ $[kg/m^3]$ is the sorption capacity of the material.

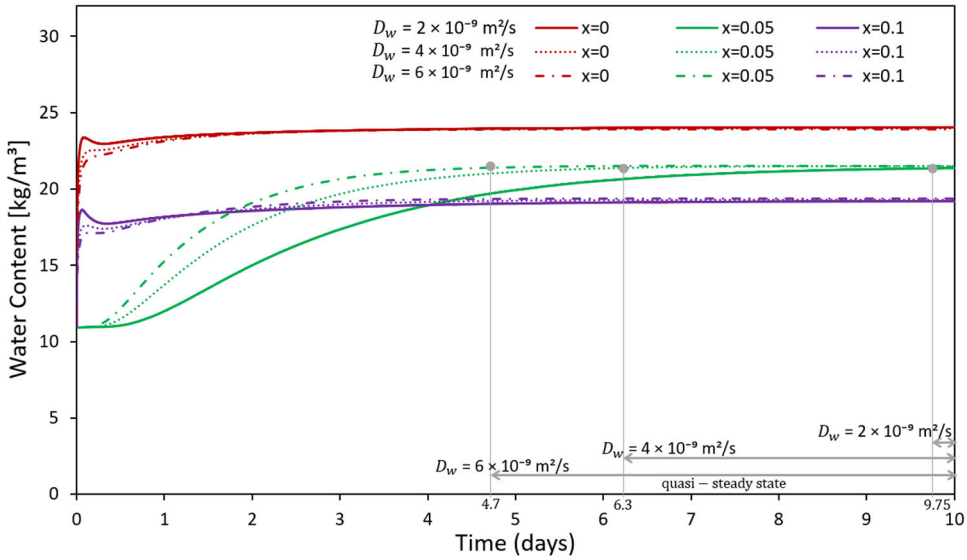


Figure 12. Influence of diffusion coefficient on the moisture response of structural material.

3.4.2. Influence of Sorption Capacity on Thermo-Hygric Behavior

Figure 13 shows the effect of variations in sorption capacity on the hygric response. It highlights the clear difference in the overall water content, and a slight difference in the diffusion kinetics as well. As with the diffusion coefficient, three values of sorption capacity were tested. Case 1 represents the actual sorption capacity of the structural material, which is the derivative of the water content with respect to relative humidity. For comparison purposes, this parameter was decreased by 50% for Case 2 and increased by 50% for Case 3. The curves show that when sorption capacity increases, the equilibrium value of water content rises, and the material needs more time to stabilize. The water content varies between 5 and 13 kg/m^3 for Case 2, 12 and 23 kg/m^3 for the reference Case 1, and 17 and 36 kg/m^3 for Case 3.

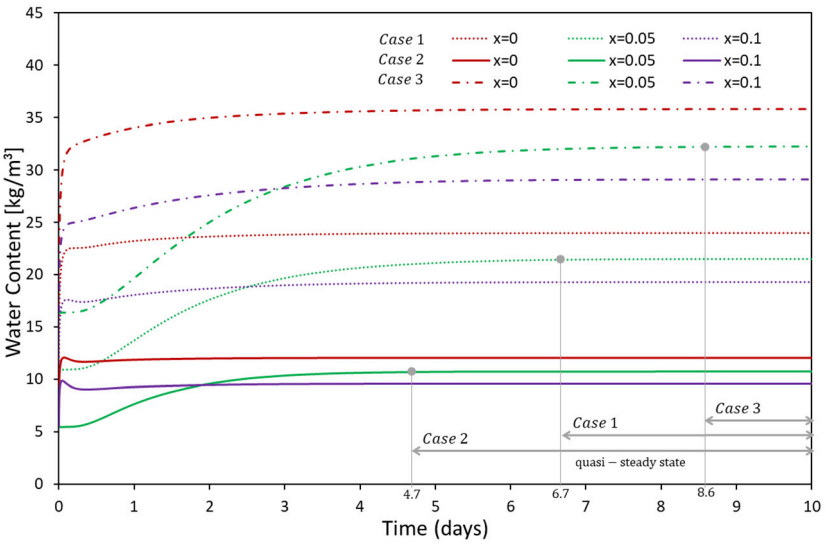


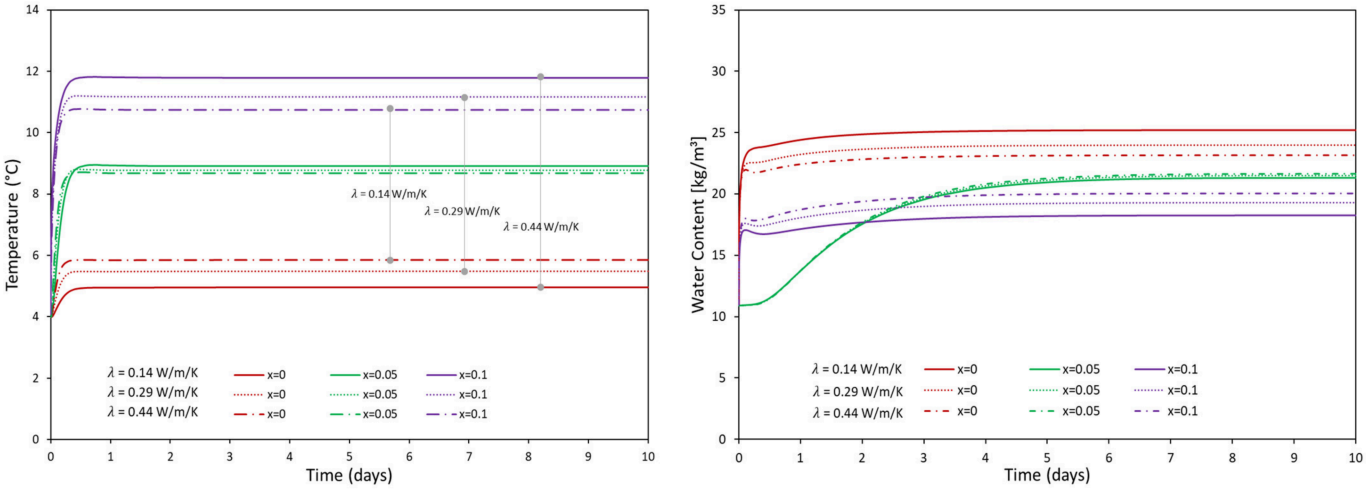
Figure 13. Influence of sorption capacity on the moisture response of structural material.

Sorption capacity represents the sensitivity of the material's water content to changes in relative humidity, which explains why, when it increases, the water content increases. Consequently, the material's moisture inertia increases when the sorption capacity increases, which prolongs the time required to reach a steady state. The stabilization time increased

from 4.7 days to 8.6 days, an increase of nearly 83%, indicating that a decrease in sorption capacity promotes faster hygric stabilization.

3.4.3. Influence of Thermal Conductivity on Thermo-Hygric Behavior

The sensitivity study of thermal conductivity for the three values considered shows, first, regarding the temperature distribution in Figure 14, that the higher the thermal conductivity, the smaller the overall temperature variation across the thickness. The gray lines show, for example, that for 0.14 W/m/K, the temperature varies between 5 °C on the exterior and 11.73 °C on the interior surface. However, for the reference thermal conductivity of 0.29 W/m/K, it varies between 5.5 °C and 11.13 °C. This means that the more conductive the material, the more homogeneous the gradient.



(**a**) (**b**)

Figure 14. Influence of thermal conductivity on (**a**) temperature and (**b**) water content distribution of the structural material.

Regarding the water content distribution in Figure 14, the diffusion time across the material is nearly identical for the three cases. On the other hand, minor variations were observed in the equilibrium values, due to the indirect relationship between thermal conductivity and sorption capacity, where a higher conductivity homogenizes the temperature gradients, which modifies the saturation vapor pressure $P_{sat}(T)$ and thus influences the rate of accumulation.

The previous interpretations highlight the following principle: sorption capacity determines the equilibrium level, and transport parameters such as the diffusion coefficient control the time of diffusion of humidity, while thermal conductivity affects the temperature field and therefore indirectly modifies local relative humidity and moisture accumulation through the temperature dependence of saturation vapor pressure. The sorption capacity is the dominant parameter for the final water content, where a $\pm 50\%$ variation in sorption capacity induces a nearly proportional $\pm 50\%$ variation in water content at the center point (0.05 m) and a $\approx 30\%$ change in the stabilization time, confirming that this parameter governs the amount of water stored at equilibrium. In contrast, water vapor permeability and thermal conductivity have only a minimal influence on the final water content, with variations of less than 0.9% for a $\pm 50\%$ change in these parameters. Water vapor permeability primarily affects the transient dynamics, where a 50% reduction in water vapor permeability extends the stabilization time by +55%, while a 50% increase reduces this time by -25%.

The results obtained from the parametric decomposition provide a better understanding of the differences in behavior identified between the three materials studied in this work. The structural material, with its higher diffusivity, allows faster moisture diffusion but stores less. The insulation material, with a lower diffusivity coefficient (1.44×10^{-9} m^2/s) than the structural material (4.09×10^{-9} m^2/s) but a greater sorption capacity and porosity, promotes greater capillary adsorption and absorption, leading to greater water storage and slower diffusion. Yet it remains effective and acts as a good buffer compared to concrete, which combines lower permeability and intermediate sorption capacity, and with its high thermal conductivity, causes faster heat transfer, but slow vapor migration, promoting interstitial moisture accumulation on the cold side. These results demonstrate the greater efficiency of bio-based earthen materials in comparison with conventional concrete.

4. From Material Scale to Building Scale: Energy Simulation of the Raw Earth Prototype Using TRNSYS

The materials' observed behaviors will have a direct effect on the overall thermal performances of real buildings. In fact, transport and storage properties govern the coupled heat–moisture transfer through walls, influencing the internal climatic conditions of a building and thus the occupant comfort. A transition to numerical modeling through TRNSYS allows the evaluation of the differences in energy performance due to the intrinsic differences between the building materials.

As part of the CobBauge project, the structural cob and the insulation light earth were tested in a real-scale prototype built in Normandy, France, where the climate is a humid oceanic climate with low temperatures. This prototype, with a surface of 13 m^2, was designed as a test cell in order to evaluate the thermal, hygrometric, and structural performances of the double-layer walls under real climatic conditions (Figure 15).



Figure 15. The building prototype under construction.

The walls are composed of an internal layer of the structural material, providing load-bearing capacity and hygrothermal regulation before encountering the interior environment. The external layer is made of the insulation material, acting as a thermal insulator and hygrometric regulator. The more porous outer insulating layer buffers variations in humidity and temperature, while the denser inner layer stores heat and regulates vapor transfer to the interior.

Figure 16 presents the building prototype modeled using SketchUp and then implemented in TRNSYS 18, a software dedicated to studying the thermal behavior of transient

systems. It is used to recreate experimental conditions and simulate the building's thermal performance. Once implemented, the model is represented as a diagram composed of several components called "Types" interlinked with each other. Each Type corresponds to a specific element of the system: the thermal simulation of the building under study is carried out by Type 56, Type 15 is used to integrate meteorological data usually generated from software such as Meteonorm 7.3, Type 9 is used to read external data files, and Type 65 is used to display and print results.

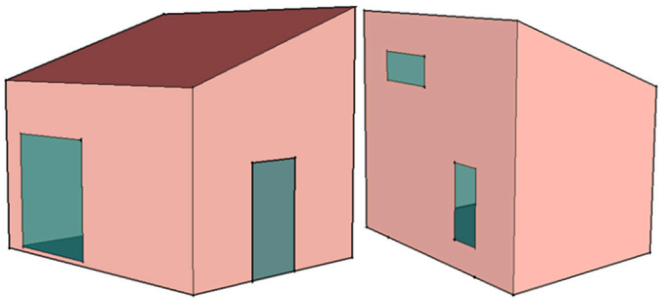


Figure 16. Three-dimensional representation of the building prototype in SketchUp.

Real meteorological data, including temperature and humidity, from the prototype's location in Normandy, France, were imported into TRNSYS, which ensures more accurate results. The study site is classified as Cfb (temperate oceanic climate) according to the Köppen–Geiger classification, characterized by mild temperatures throughout the year, the absence of a dry season, and cool summers. The building characteristics were then specified in Type 56. Each wall was defined layer by layer, specifying for each material its thickness, thermal conductivity, heat capacity and density.

4.1. Comparative Analysis Between Cob and Conventional Materials

To determine the energy performance of the building under study, heating and cooling demands were simulated using TRNSYS software. These calculations are based on a comfort temperature range defined between 19 °C and 26 °C, as stipulated in articles R241-26 and R241-30 of the French Energy Code [46]. In the absence of a specific legal text governing the heating period, it is generally set as between October 15 and April 15. However, this period may differ according to the region, the local climatic conditions, and the policies or regulations established by local authorities or building managers. For the purposes of this study, this period was used as a reference for the analysis.

The assumptions used in the simulations are as follows:

- The infiltration rate is fixed at 0.6 air changes per hour.
- No mechanical ventilation or internal gains are taken into account.
- The prototype is maintained at 19 °C during occupied hours and at 12 °C during unoccupied periods.
- The cooling setpoint is set to 26 °C.

This analysis allowed us to compare the energy performance of two prototypes: one built from cob and the other from conventional materials. Table 5 illustrates the composition of the structural elements of these two prototypes, highlighting the differences in the materials used. In order to ensure a reliable comparison between the cob and conventional buildings, both share identical floor and roof configurations, differing only in their external wall composition. This approach isolates the thermal contribution of the wall system. The thermal transmittance (U-value) of the cob wall ranges between 0.232 W/m^2K for the West and South walls and 0.290 W/m^2K for the East and North walls due to thickness variations. While the conventional wall yields a value of 0.262 W/m^2K. These values are comparable,

confirming that the two prototypes operate under thermally equivalent envelope conditions. Furthermore, both prototypes were assigned identical solar orientations. Window openings, with a U-value of 2.95 W/m^{2}K, were placed on the south-facing wall, with a total glazed area of 4.80 m^2, representing the largest opening to maximize solar gains during winter. Two additional smaller windows were placed on the north facade (1.1 m^2 and 0.9 m^2).

After simulating with TRNSYS, the results show a heating demand for both prototypes, but no cooling demand, which can be explained by the cold climate of the region studied. Figure 17 shows that the heating energy demand for the year 2023 is higher for the conventional prototype for the entire heating period, with a total of 79 kWh/m^2/year, than for the cob prototype, with a total of 60 kWh/m^2/year. These results demonstrate the better energy performance of the cob prototype, which can be attributed to the ability of bio-based materials to store and slowly release heat, thus reducing thermal fluctuations inside the building. To summarize, this comparison illustrates that buildings incorporating bio-based materials, such as cob, offer a high-performance, sustainable alternative to conventional construction. These results reinforce the promotion of the use of these materials in the building sector, with the goal of reducing energy consumption and the associated environmental impacts.

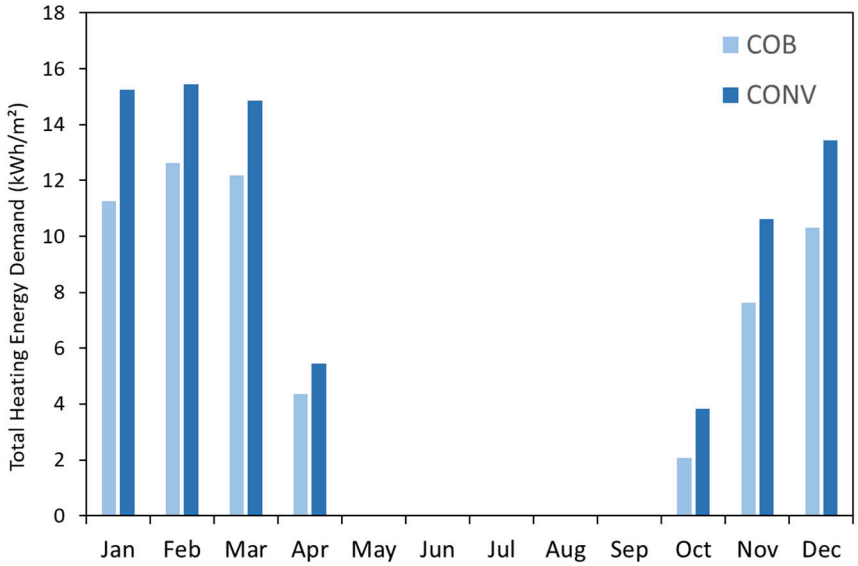


Figure 17. Total heating energy demand in 2023 for the cob and conventional prototypes.

Table 5. Structural composition of cob and conventional prototypes.

Building Component		Composition	Thermal Resistance (m^2.K/W)	Thickness (mm)	
				E-N	S-W
External Wall	COB building	Lime	0.010	20	
		Cob_Structural	0.841 [25 cm]	450	250
		Cob_Insulation	2.404 [25 cm]	270	250
		Coated raw earth	0.027	20	
	Conventional building	Plasterboard	0.052	13	
		Rockwool	3.191	150	
		Concrete blocks	0.385	200	
		Exterior mortar plaster	0.012	15	

Table 5. *Cont.*

Building Component	Composition	Thermal Resistance (m^2.K/W)	Thickness (mm)	
			E-N	S-W
Floor	Reinforced concrete slab	0.114	200	
	Expanded cork insulation	0.250	10	
	Rammed earth finishing slab	0.091	100	
Ceiling	Corrugated steel roofing sheets	0.000	18	
	Wood	0.252	58	
	Wood fiber rain barrier	0.400	22	
	Wood fiber insulation	7.500	300	
	Polyethylene vapor barrier	0.003	1	
	Wood	0.039	9	

4.2. Energy Demand Analysis of the Cob Prototype Across Climate Zones

This section compares the heating and cooling requirements for the cob prototype in the three climatic zones of France. This classification is based on the French Thermal Regulations (RT). The city of Dijon was chosen as the cold climate zone, marked by cold winters and moderate summers, classified as Cfb. Saint-Lô, located in Normandy, was selected as the temperate and humid climate zone because of the location of the prototype under study in this zone, enabling direct experimental evaluation of the building performance. Nice was chosen to represent the Mediterranean climate zone (Csa), known for its hot, dry summers and mild winters, which enables the assessment of the cob prototype's ability to regulate temperature and limit air-conditioning requirements.

Figure 18 illustrates outdoor (dark blue bars) and indoor (light blue bars) temperature ranges for the three cities, highlighting the temperature regulation capabilities of the cob prototype. The results show that Nice has the highest outdoor temperatures, ranging from 3 °C to 36 °C over the course of the year. Dijon has the widest temperature range, with a minimum of −6.5 °C and a maximum of 36 °C. And Saint-Lô shows outdoor temperatures ranging from −5 °C to 31 °C. Inside the cob prototype, the figure shows a significant reduction in temperature fluctuations due to the thermal properties of the cob materials. The variations recorded for Nice are between 8 °C and 28 °C, showing better protection against heat peaks. For Dijon, despite its harsh winter, the indoor temperatures were regulated between 4 °C and 25 °C, which is also the case for Saint-Lô, with temperatures ranging from 5 °C to 21 °C. These results confirm that the cob material acts as a thermal buffer, limiting extreme variations and promoting a stable, comfortable indoor environment regardless of the climatic conditions outside.

The simulation results presented in Figure 19 show that the heating demand is higher in cities with a cold climate (Dijon) and a humid climate (Saint-Lô), where winters are colder, with a total energy demand for the cold climate of 74 kWh/m^2/year and 60 kWh/m^2/year for the humid and temperate climate. Meanwhile, for the Mediterranean climate, a lower demand of 42 kWh/m^2/year is obtained. Regarding cooling, in Dijon and Saint-Lô, there is no cooling requirement, reflecting their cold summers. On the other hand, Nice, which experiences hot summers, shows a moderate cooling demand, mainly over a few days in July, August, and September, with a total of 1.5 kWh/m^2/year. These low cooling requirements demonstrate the cob prototype's effectiveness in limiting indoor temperature peaks despite harsh outdoor climatic conditions.

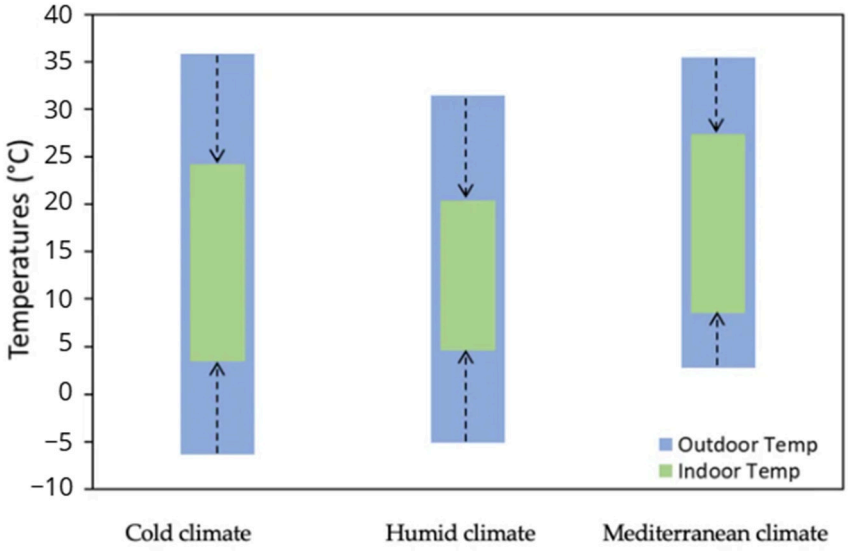


Figure 18. Thermal regulation: Indoor vs. outdoor temperatures in the three climatic zones. (Cold climate = Dijon, Humid climate = Saint-Lô, Mediterranean climate = Nice).

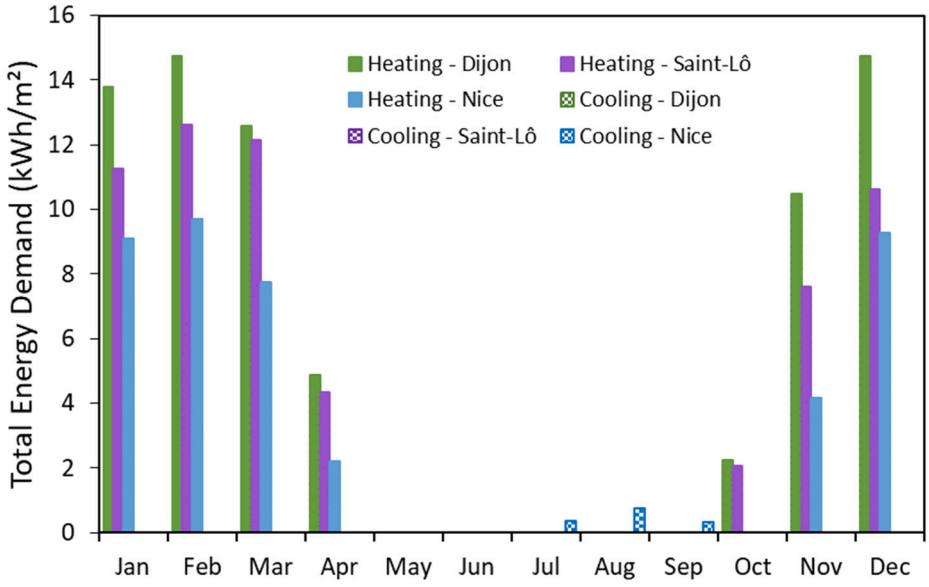


Figure 19. Total heating and cooling energy demand in 2023 for Dijon, Saint-Lô, and Nice.

These observations highlight the ability of cob construction to effectively regulate indoor temperatures, reducing discrepancies between minimum and maximum temperatures. This underlines the effectiveness of bio-based materials as a high-performance alternative for limiting energy requirements across a variety of climatic contexts. Furthermore, the results demonstrate that the local climate has a significant influence on the energy performance of buildings, underlining the importance of taking regional climatic conditions into account when designing constructions using natural materials.

5. Conclusions

This article establishes a clear link between the hygrothermal behavior of the bio-based earthen materials studied at the material scale and the overall energy performance observed at the building scale through a combined experimental and numerical approach, contributing to the hygrothermal characterization of bio-based earthen construction materials. The results highlighted the remarkable ability of cob materials to regulate temperature

and humidity, thanks to their high thermal inertia and their ability to absorb and release water vapor. Their MBV values further confirmed their good buffering behavior, with 2.23 ± 0.032 g/(m^2·%RH) for the structural material and 1.21 ± 0.017 g/(m^2·%RH) for the insulation. The sorption isotherm characterization revealed a reduction of 26% in sorption capacity between 23 °C and 45 °C for both materials, demonstrating the self-regulating properties of soil–fiber materials, where, in summer conditions or in heated spaces, these materials naturally release previously stored moisture, thereby contributing to the passive regulation of indoor humidity on a seasonal basis.

Their performance depends strongly on key parameters such as thermal conductivity, sorption capacity, porosity, and diffusion coefficient. Sensitivity studies demonstrated that the bio-based materials studied outperform conventional concrete under severe winter conditions, not only because of their thermal conductivity, whose influence on the final moisture content is less than 0.9%, but also due to the combination of their high sorption capacity and their porous structure. Moisture diffusivity emerges as the key parameter in transient dynamics: at 4.09×10^{-9} m^2/s for the structural material and 1.44×10^{-9} m^2/s for the insulation, it governs the rate of moisture equilibration, with the stabilization time varying from 4.7 to 9.75 days depending on vapor permeability. In contrast, concrete, combining low vapor permeability with high thermal conductivity, promotes interstitial moisture accumulation.

These properties, observed during sample testing, translate directly to the prototype scale in the form of a significant reduction in indoor temperature fluctuations and improved hygrothermal comfort. During the heating period, the energy requirements for the cob building showed a decrease of 24%, reflecting its good thermal performance. These results help address the lack of quantitative data on local earthen materials and provide validated input data for hygrothermal simulations, paving the way for the broader integration of these materials into sustainable construction practices in France and Europe.

Author Contributions: Conceptualization, H.L., K.S. and Y.T.; methodology, K.S., Y.T. and H.L.; software, K.S.; validation, K.S.; formal analysis, K.S., H.L., I.V., A.-L.T. and M.M.; investigation, K.S., H.L., I.V., M.M. and A.-L.T.; resources, K.S., M.M., A.-L.T., I.V. and H.L.; data curation, K.S.; writing—original draft preparation, K.S. and Y.T.; writing—review and editing, K.S., H.L., M.M., I.V. and A.-L.T.; supervision, H.L.; project administration, H.L. All authors have read and agreed to the published version of the manuscript.

Funding: This paper is an extension work of the study conducted under the CobBauge project selected by the European cross-border cooperation program INTERREG V France (Manche)-England. The authors would like to thank the ERDF for the funding of this work.

Data Availability Statement: The data presented in this study is available on request from the corresponding author due to privacy.

Conflicts of Interest: The authors declare no conflicts of interest.

Appendix A

The temperature equation used in COMSOL Multiphysics is the classic convection–diffusion equation, taking into account the solid matrix, liquid water, and moist air properties, and is valid when all phases share the same local temperatures (thermal equilibrium $T_{fluid} = T_{solid} = T$) [47]. This equation is written as

$$\left(\rho C_p\right)_{eff} \frac{\partial T}{\partial t} + \left(\rho_g C_{p,g} u_g + \rho_l C_{p,l} u_l\right) \cdot \nabla T + \nabla \cdot q = \mathrm{Q} + Q_{evap} \tag{A1}$$

with

$$q = -d_z k_{eff} \nabla T \tag{A2}$$

$$(\rho C_p)_{eff} = \theta_s \rho_s C_{p,s} + \varepsilon_p \left[(1 - s_l) \rho_g C_{p,g} + s_l \rho_l C_{p,l} \right] \quad \text{(A3)}$$

The three-phase porous domain is described by volume fractions θ_s and porosity ε_p, with a liquid water saturation s_l, which represents the fraction of the pore volume occupied by liquid water; it varies between 0 and 1, influencing the effective thermal and hydraulic properties of the material. ρ_g and ρ_l [kg/m^3] represent the moist air and liquid water densities, $C_{p,g}$ and $C_{p,l}$ [J/(kg·K)] are the moist air and liquid water heat capacities at constant pressure, $(\rho C_p)_{eff}$ [J/(m^3·K)] is the effective volumetric heat capacity at constant pressure, taking into account the solid matrix, the moist air, and the liquid water properties, q [W/m^2] represents the conductive heat flux, u_g and u_l [m/s] are the moist air velocity field and the liquid water velocity field, respectively, k_{eff} [W/(m·K)] is the effective thermal conductivity, and Q and Q_{evap} [W/m^3] are respectively the sum of the diffusive flux of enthalpy and of the liquid capillary flux and the heat source.

The equation for the transport of the total moisture can be written as Equation (A4), combining transfer by liquid transport (capillary and convective flux), and vapor convection and diffusion.

$$d_z \frac{\partial w(\phi_w)}{\partial t} + d_z \rho_g u_g \cdot \nabla \omega_v + \nabla \cdot g_w + d_z u_l \cdot \nabla \rho_l + d_z \nabla \cdot g_{lc} = d_z G \quad \text{(A4)}$$

with

$$w(\phi_w) = \epsilon_p \left(\rho_l s_l + \rho_g \omega_v (1 - s_l) \right) \quad \text{(A5)}$$

where $w(\phi_w)$ [kg/m^3] is the total moisture content, φ_w is the relative humidity, ρ_g [kg/m^3] is the moist air density, ω_v represents the vapor mass fraction in moist air, g_w is the moisture diffusive flux, g_{lc} is the liquid water capillary flux, and G [kg/(m^3·s)] represents a moisture source.

References

1. Santamouris, M.; Vasilakopoulou, K. Present and future energy consumption of buildings: Challenges and opportunities towards decarbonisation. *e-Prime—Adv. Electr. Eng. Electron. Energy* **2021**, *1*, 100002. [CrossRef]
2. United Nations Environment Programme. *Global Status Report for Buildings and Construction*; United Nations Environment Programme: Nairobi, Kenya, 2020; Volume 10. Available online: https://globalabc.org/sites/default/files/inline-files/2020%20Buildings%20GSR_FULL%20REPORT.pdf (accessed on 16 May 2026).
3. Cosentino, L.; Fernandes, J.; Mateus, R. Fast-growing bio-based construction materials as an approach to accelerate United Nations Sustainable Development Goals. *Appl. Sci.* **2024**, *14*, 4850. [CrossRef]
4. Rosa Latapie, S.; Abou-Chakra, A.; Sabathier, V. Microstructure of bio-based building materials: New insights into the hysteresis phenomenon and its consequences. *Buildings* **2023**, *13*, 1650. [CrossRef]
5. Wildman, J.; Shea, A.; Cascione, V.; Henk, D. Mould susceptibility of bio-based insulation materials in modern construction. *npj Mater. Degrad.* **2026**, *10*, 29. [CrossRef]
6. Rosa Latapie, S.; Abou-Chakra, A.; Sabathier, V. Bibliometric analysis of bio- and earth-based building materials: Current and future trends. *Constr. Mater.* **2023**, *3*, 474–508. [CrossRef]
7. Kulshreshtha, Y.; Mota, N.J.A.; Jagadish, K.S.; Bredenoord, J.; Vardon, P.J.; van Loosdrecht, M.C.M.; Jonkers, H.M. The potential and current status of earthen material for low-cost housing in rural India. *Constr. Build. Mater.* **2020**, *247*, 118615. [CrossRef]
8. Touati, K.; Benzaama, M.-H.; El Mendili, Y.; Le Guern, M.; Streiff, F.; Goodhew, S. Hygrothermal and economic analysis of an earth-based building using in situ investigations and artificial neural network modeling for Normandy's climate conditions. *Sustainability* **2023**, *15*, 13985. [CrossRef]
9. Hamard, E.; Cazacliu, B.; Razakamanantsoa, A.; Morel, J.-C. Cob, a vernacular earth construction process in the context of modern sustainable building. *Build. Environ.* **2016**, *106*, 103–119. [CrossRef]
10. Ben-Alon, L.; Rempel, A.R. Thermal comfort and passive survivability in earthen buildings. *Build. Environ.* **2023**, *238*, 110339. [CrossRef]
11. Zeghari, K.; Gounni, A.; Louahlia, H.; Marion, M.; Boutouil, M.; Goodhew, S.; Streiff, F. Novel dual walling cob building: Dynamic thermal performance. *Energies* **2021**, *14*, 7663. [CrossRef]

12. Laborel-Préneron, A.; Magniont, C.; Aubert, J.-E. Hygrothermal properties of unfired earth bricks: Effect of barley straw, hemp shiv and corn cob addition. *Energy Build.* **2018**, *178*, 265–278. [CrossRef]
13. Nguyen, Q.V.; Djedjig, R.; Rahim, M.; Tran-Le, A.D.; Hoang, D.Q.; Gao, Z.; Nguyen, M.L.; Bui, Q.B.; Nguyen, D.M. Impact of hemp shiv contents on hygrothermal and compressive properties of raw earth-based sustainable building materials. *J. Aust. Ceram. Soc.* **2026**, 1–15. [CrossRef]
14. Alioui, A.; Idrissi Kaitouni, S.; Azalam, Y.; Al Armouzi, N.; Bendada, E.M.; Mabrouki, M. Effect of straw fibers addition on hygrothermal and mechanical properties of carbon-free adobe bricks: From material to building scale in a semi-arid climate. *Build. Environ.* **2024**, *255*, 111380. [CrossRef]
15. Gowthaman, S.; Nakashima, K.; Kawasaki, S. A state-of-the-art review on soil reinforcement technology using natural plant fiber materials: Past findings, present trends and future directions. *Materials* **2018**, *11*, 553. [CrossRef] [PubMed]
16. Kabore, A.; Ouellet-Plamondon, C.M. Improved insulation with fibres in heavy cob for building walls. *Ind. Crops Prod.* **2024**, *215*, 118626. [CrossRef]
17. Shon, C.-S.; Mukashev, T.; Lee, D.; Zhang, D.; Kim, J.R. Can common reed fiber become an effective construction material? Physical, mechanical, and thermal properties of mortar mixture containing common reed fiber. *Sustainability* **2019**, *11*, 903. [CrossRef]
18. Gounni, A.; Louahlia, H. Dynamic behavior and economic analysis of sustainable building integrating cob and phase change materials. *Constr. Build. Mater.* **2020**, *262*, 120795. [CrossRef]
19. Touati, K.; Le Guern, M.; El Mendili, Y.; Azil, A.; Streiff, F.; Carfrae, J.; Fox, M.; Goodhew, S.; Boutouil, M. Earthen-based building: In-situ drying kinetics and shrinkage. *Constr. Build. Mater.* **2023**, *369*, 130544. [CrossRef]
20. Carcassi, O.B.; Salierno, R.; Falcinelli, P.A.; Paoletti, I.M.; Ben-Alon, L. Upscaling natural materials in construction: Earthen, fast-growing, and living materials. *Sustainability* **2024**, *16*, 7926. [CrossRef]
21. Brinkmann, M.; Wiehle, P. Correlation between relative humidity and the strength and deformation characteristics of unstabilised earth masonry. *Constr. Build. Mater.* **2023**, *366*, 130048. [CrossRef]
22. Lourenço, P.B.; Luso, E.; Almeida, M.G. Defects and moisture problems in buildings from historical city centres: A case study in Portugal. *Build. Environ.* **2006**, *41*, 223–234. [CrossRef]
23. Xue, Y.; Fan, Y.; Chen, S.; Wang, Z.; Gao, W.; Sun, Z.; Ge, J. Heat and moisture transfer in wall-to-floor thermal bridges and its influence on thermal performance. *Energy Build.* **2022**, *278*, 112642. [CrossRef]
24. Wolkoff, P. Indoor air humidity, air quality, and health—An overview. *Int. J. Hyg. Environ. Health* **2018**, *221*, 376–390. [CrossRef] [PubMed]
25. Psomas, T.; Teli, D.; Langer, S.; Wahlgren, P.; Wargocki, P. Indoor humidity of dwellings and association with building characteristics, behaviors and health in a northern climate. *Build. Environ.* **2021**, *198*, 107885. [CrossRef]
26. Cristaudo, A.; Nicoletti, F.; Carpino, C.; Bruno, R. Dynamic Hygrothermal Analysis for Retrofitting Opaque Envelopes in Humid Climates: From Simulations to Guidelines. *Buildings* **2026**, *16*, 419. [CrossRef]
27. Bucklin, O.; Müller, T.; Amtsberg, F.; Leistner, P.; Menges, A. Analysis of thermal transmittance, air permeability, and hygrothermal behavior of a solid timber building envelope. *Energy Build.* **2023**, *299*, 113629. [CrossRef]
28. Osanyintola, O.F.; Simonson, C.J. Moisture buffering capacity of hygroscopic building materials: Experimental facilities and energy impact. *Energy Build.* **2006**, *38*, 1270–1282. [CrossRef]
29. Viitanen, H.; Vinha, J.; Salminen, K.; Ojanen, T.; Peuhkuri, R.; Paajanen, L.; Lähdesmäki, K. Moisture and bio-deterioration risk of building materials and structures. *J. Build. Phys.* **2010**, *33*, 201–224. [CrossRef]
30. Giada, G.; Caponetto, R.; Nocera, F. Hygrothermal properties of raw earth materials: A literature review. *Sustainability* **2019**, *11*, 5342. [CrossRef]
31. Kaoutari, H.; Louahlia, H. Experimental and numerical investigations on the thermal and moisture transfer in green dual layer wall for building. *Case Stud. Therm. Eng.* **2024**, *48*, 103946. [CrossRef]
32. Kaoutari, T.; Louahlia, H.; Schaetzel, P.; Lepinasse, E.; Boutouil, M.; Goodhew, S.; Streiff, F. Hygric properties and adsorption characteristics of simple and dual cob layers of bio-sourced building materials. *Constr. Build. Mater.* **2023**, *403*, 133157. [CrossRef]
33. Sidqui, K.; Taouirte, Y.; Zeghari, K.; Voicu, I.; Tiffonnet, A.-L.; Marion, M.; Louahlia, H. Thermal and Hygric Behavior of Bio-Based Building Dual Walls. *Buildings* **2026**, *16*, 83. [CrossRef]
34. Xue, Y.; Fan, Y.; Wang, Z.; Gao, W.; Sun, Z.; Ge, J. Facilitator of moisture accumulation in building envelopes and its influences on condensation and mould growth. *Energy Build.* **2022**, *277*, 112528. [CrossRef]
35. CobBauge Project, Soil and Fibre Characterisation, Mixes Choice and Mixes Characteristics. Available online: http://www.cobbauge.eu/wp-content/uploads/2019/05/Technical-report_ESITC_feb2019.pdf (accessed on 4 February 2026).
36. Rode, C.; Peuhkuri, R.H.; Hansen, K.K.; Time, B.; Svennberg, K.; Arfvidsson, J.; Ojanen, T. NORDTEST project on moisture buffer value of materials. In *AIVC 26th Conference: Ventilation in Relation to the Energy Performance of Buildings*; INIVE EEIG: Ghent, Belgium, 2005; pp. 47–52.

37. Khaled, S.; Collet, F.; Prétot, S.; Bart, M. Effect of air velocity and initial conditioning on the moisture buffer value of four different building materials. *Materials* **2023**, *16*, 3284. [CrossRef] [PubMed]
38. Abdellatef, Y.; Khan, M.A.; Khan, A.; Alam, M.I.; Kavgic, M. Mechanical, thermal, and moisture buffering properties of novel insulating hemp-lime composite building materials. *Materials* **2020**, *13*, 5000. [CrossRef] [PubMed]
39. Larcher, M.; Leonardi, E.; Troi, A.; Stefani, A.; Nerobutto, G.; Herrera-Avellanosa, D. Assessing the impact of moisture buffering properties of materials on indoor environmental quality: A study on a recycled material plaster. *Build. Environ.* **2025**, *267*, 112170. [CrossRef]
40. Rode, C.; Grau, K. Moisture buffering and its consequence in whole building hygrothermal modeling. *J. Build. Phys.* **2008**, *31*, 333–360. [CrossRef]
41. Collet, F.; Chamoin, J.; Pretot, S.; Lanos, C. Comparison of the hygric behaviour of three hemp concretes. *Energy Build.* **2013**, *62*, 294–303. [CrossRef]
42. Mazhoud, B.; Collet, F.; Prétot, S.; Lanos, C. Effect of hemp content and clay stabilization on hygric and thermal properties of hemp-clay composites. *Constr. Build. Mater.* **2021**, *300*, 123878. [CrossRef]
43. Ranefjärd, O.; Strandberg-de Bruijn, P.B.; Wadsö, L. Hygrothermal properties and performance of bio-based insulation materials locally sourced in Sweden. *Materials* **2024**, *17*, 2021. [CrossRef] [PubMed]
44. Chehade, S.; Dujardin, N.; Duc, M.; Keita, E.; Boudenne, A. Advanced investigation of water sorption isotherms measured on raw earth construction blocks. *Mater. Struct.* **2026**, *59*, 236. [CrossRef]
45. *EN 15026:2023*; Hygrothermal Performance of Building Components and Building Elements—Assessment of Moisture Transfer by Numerical Simulation. CEN: Brussels, Belgium, 2023.
46. Legifrance. Livre II: La Maîtrise de la Demande d'Energie et le Développement des Energies Renouvelables (Articles D211-1 à R293-1). Code de L'énergie. Available online: https://www.legifrance.gouv.fr/codes/section_lc/LEGITEXT000023983208/LEGISCTA000031748103/#LEGISCTA000031748103 (accessed on 30 December 2025).
47. COMSOL AB. *Heat Transfer Module User's Guide (Version 5.5); COMSOL Documentation*; COMSOL AB: Stockholm, Sweden, 2019. Available online: https://doc.comsol.com/5.5/doc/com.comsol.help.heat/heat_ug_theory.07.14.html#638569 (accessed on 24 January 2026).

Disclaimer/Publisher's Note: The statements, opinions and data contained in all publications are solely those of the individual author(s) and contributor(s) and not of MDPI and/or the editor(s). MDPI and/or the editor(s) disclaim responsibility for any injury to people or property resulting from any ideas, methods, instructions or products referred to in the content.